LA-UR-17-29521 (Accepted Manuscript)

Ultra-high-bandwidth polarization interferometry and optimal quadratic phase detection

Weber, Thomas
Smith, Roger

To be published in: Review of Scientific Instruments

DOI to publisher's version: 10.1063/1.5091569

Permalink to record: http://permalink.lanl.gov/object/view?what=info:lanl-repo/lareport/LA-UR-17-29521

Ultra-high-bandwidth polarization interferometry and optimal quadratic phase detection

T.E. Weber[1, a)] and R.J. Smith[2]

[1)] *Physics Division, Los Alamos National Laboratory, P.O. Box 1663, Los Alamos, NM 87545, USA*

[2)] *TAE Tecnnologies Inc., 19631 Pauling, Foothill Ranch, CA 92610, USA*

(Dated: 10 June 2019)

A novel homodyne interferometer and analysis method are described which use orthogonal polarization components to measure large rapid changes in interferometric phase, in quadrature, in the presence of strong time-dependent attenuation of the scene beam. This approach overcomes the major sources of error associated with homodyne interferometry (sensitivity nulls, ambiguity in the direction of phase change when passing through a sensitivity null, and intolerance to beam power variations) while maintaining its intrinsic simplicity and speed; enabling extremely high-bandwidth, high-dynamic range measurements limited only by available detector technology. Using this technique, electron density in a magnetized plasma shock was measured with unprecedented bandwidth and resolution, revealing short-timescale features not previously observed.

PACS numbers: 07.60.Ly (Interferometers), 42.25.Ja (Polarization in wave optics), 06.60.Jn (High-speed techniques)

I. INTRODUCTION

Optical interferometry is used in a wide range of applications to measure changes in distance or refractive index. However, large changes in interferometric phase and beam power variations are common in many systems, and resolving complex dynamics at bandwidths greater than tens of megahertz in these cases requires quadratic measurement of phase over much shorter timescales than can be achieved using existing techniques.

Homodyne interferometry[1], in which two identical beams are combined to produce interference on a single detector, is a simple technique capable of essentially unlimited bandwidth but has three major sources of error:

1. Sensitivity nulls when the phase difference, ϕ, between the interfering beams is near $n\pi$, where n is an integer
2. Ambiguity in the sign of $\mathrm{d}\phi/\mathrm{d}t$ when ϕ crosses a sensitivity null
3. Beam power variations, due to refraction or attenuation of the scene beam or laser power fluctuations, can be misinterpreted as phase shifts

Heterodyne interferometry[1] avoids these issues by modulating the phase of the reference or scene beam, typically via acousto-optic modulation at 40 or 80 MHz (but sometimes by more cumbersome methods[2,3]), and mixing the detected intensity signal of the recombined beams with the local oscillator signal using an in-phase quadrature (IQ) demodulator. The outputs of the IQ demodulator are proportional to $\sin\phi$ and $\cos\phi$, enabling phase to be measured in quadrature independently of the intensities of the scene and reference beams (provided that the modulation frequency is much higher than any frequency component of ϕ being measured). While this approach has been highly successful (e.g., heterodyne interferometry is widely used to infer the density of magnetized plasmas in laboratory experiments[4]), it requires the use of additional radio-frequency hardware and substantially limits measurement bandwidth.

Measuring high-speed dynamics, such as those present in moderate to high-energy-density plasmas, often requires resolving phase changes over much shorter timescales than can be achieved using heterodyne techniques. Typically in these situations, homodyne systems are used that are designed to operate at low levels of phase shift; i.e., $\phi < \pi$ (e.g., by using a shorter wavelengths laser to decrease sensitivity to plasma density[4]). This avoids issues 1 and 2 but often reduces the dynamic range of the measurement to unacceptably low levels, a situation that is often exacerbated by high levels of electromagnetic interference (EMI) present during plasma discharges. Increasing the dynamic range by using longer wavelengths to produce larger phase shifts ($\phi > \pi$) makes the system susceptible to issues 1 and 2 and is also often associated with high levels of refraction and/or attenuation of the scene beam, leading to issue 3.

To overcome these limitations, an interferometer was developed that uses orthogonal polarization components to effectively form two homodyne interferometers along the same optical path. By introducing a relative phase shift (in this case, $\pi/2$) between the two polarization components and by keeping track of each intensity term during the mathematical analysis (rather than combining terms, as was done in the past), interferometric phase can be computed in quadrature while taking into account variations in laser intensity and/or attenuation of the scene beam. This approach maintains the intrinsic simplicity and high-bandwidth of homodyne interferometry, while avoiding all three major sources of error listed above.

[a)] Electronic mail: tweber@lanl.gov

II. BACKGROUND

Interferometric techniques using polarization to obtain phase information have been pursued for over 50 years. Most notably, the interferometer first described by Martin and Puplett[5] in 1969 used polarizing beam splitters in a Mach-Zehnder[1] topology to produce orthogonal polarizations in the scene and reference beams. The Martin-Puplett interferometer, however, did not measure phase in quadrature and does not address the sources of error associated with homodyne interferometry listed in Sec. I.

In 1970, Boricius and Clifford[6] gave an account of an interferometer somewhat similar to the one described herein (a Mach-Zehnder topology with a circularly polarized reference beam and a non-polarizing recombining beam splitter), although they did not recognize that recombining the beams using a non-polarizing beam splitter introduces a polarization-dependent phase shift that alters the polarization state of the reflected beam, necessitating the use of additional polarization optics to condition the beams prior to recombination, as is subsequently discussed. Buchenauer and Jacobson[7] in 1977 used a similar setup to measure plasma density in an electrical discharge. While they discussed the need to condition the polarization of the beam prior to recombination, they assumed constant laser power (a reasonable assumption, if verified) and no attenuation in the scene beam (despite reporting changes in the fringe envelope during a plasma discharge, clear evidence of attenuation). In contrast, the method described in this paper accounts for intensity variations in either or both the scene and reference beams depending on the number of detectors used.

More recently, Greco et al.[8] in 1995, and later others,[9,10] described a Martin-Puplett interferometer in a Michelson topology that employed a 4-detector analyzer scheme to account for laser power variations. However, their system could not measure attenuation of the scene beam, which, in many cases, is much more important than monitoring laser power. Similar to Boricius and Clifford, they did not consider polarization-dependent phase shifts introduced during recombination. Furthermore, they made use of both outputs of their non-polarizing beam splitters; an additional complication that precludes proper polarization conditioning.

A common thread in all of these previous works is that, in their mathematical analysis, they lumped together individual intensities (e.g., s-polarized scene beam intensity) into fewer combined terms, and in doing so, were unable to recover information about the scene and reference beam intensities without using additional information (i.e., using more detectors). This can be problematic for the reasons discussed above (and expanded upon in the following sections). By avoiding this temptation, we maximize the use of information and do not require the use of both outputs of the recombining beam splitter. We present a method in which the number of detectors required is equal to the number of unknowns being measured. In this case, two detectors were used to measure two quantities during a plasma discharge: 1. interferometric phase and 2. scene beam intensity, which changes due to attenuation. However, it should be noted that two detectors are needed at a minimum to measure phase in quadrature; and the scene beam intensity (or laser stability if desired instead) can be obtained without the addition of another detector. Furthermore, using this approach, calibration of the system can be performed remotely; i.e., without disassembly (which would alter the alignment in a manner that would change the calibration) or other modification requiring the diagnostician to enter the experimental area.

III. APPARATUS AND METHODS

A simplified schematic of the interferometer and analyzer is shown in Fig. 1. A polarized laser oriented at 45° emits a beam with equal power in the s (vertical) and p (horizontal) polarization components, which is then split, using a non-polarizing beam splitter, into scene and reference beams. The reference beam passes through a $\lambda/4$ wave plate oriented so as to retard only the phase of the p-component, and the beams are recombined using a second non-polarizing beam splitter. The recombined beam is subsequently split into linear polarization states by a polarizing beam splitter and detected using silicon photodiodes. Apertures and narrow bandpass filters are placed prior to the detectors to reject the broadband plasma emission, and lenses focus the beams onto the detector elements.

Several types of non-polarizing beam splitters were tested, however, it was discovered that all exhibited a polarization-dependent splitting ratio and introduced different amounts of relative phase delay to the s and p polarization components depending on whether the beam was transmitted or reflected (see Sec. IV). Thus only one output of the recombining beam splitter could be utilized in the detection scheme. Furthermore, small changes to the state of polarization of both beams were introduced by elements such as mirrors and vacuum windows. A polarizer oriented at approximately 45° (to clean up the polarization state while preserving as much power as possible) and $\lambda/2$ wave plate (to tune the polarization angle) were placed in series with the $\lambda/4$ wave plate in the reference beam such that the reflected output of the recombining beam splitter was purely circularly polarized. Similarly, a polarizer at ∼45° (both to enforce polarization and reject approximately half of the unwanted plasma emission) and $\lambda/2$ wave plate were placed in the scene beam to ensure a pure 45° linear polarization state upon transmission through the beam splitter.

The superposed electric field of the reference (ref) and scene (scn) beams, including the phase shift, can be written as

$$\begin{aligned}\mathbf{E}(t) &= [E_{s\,\mathrm{ref}}(t) + E_{s\,\mathrm{scn}}(t)]\,\hat{\mathbf{e}}_\mathbf{s} + \\ &\quad [E_{p\,\mathrm{ref}}(t) + E_{p\,\mathrm{scn}}(t)]\,\hat{\mathbf{e}}_\mathbf{p} \qquad (1)\\ &= \mathrm{Re}\left\{\widetilde{E}_{s\,\mathrm{ref}} e^{i\theta} + \widetilde{E}_{s\,\mathrm{scn}} e^{i(\theta+\phi)}\right\}\hat{\mathbf{e}}_\mathbf{s} + \\ &\quad \mathrm{Re}\left\{\widetilde{E}_{p\,\mathrm{ref}} e^{i(\theta+\xi)} + \widetilde{E}_{p\,\mathrm{scn}} e^{i(\theta+\phi)}\right\}\hat{\mathbf{e}}_\mathbf{p} \qquad (2)\end{aligned}$$

where, for example, $\hat{\mathbf{e}}_\mathbf{s}$ is the unit vector in the s direction, $\widetilde{E}_{s\,\mathrm{scn}}$ is the modulus of the s-polarized scene beam,

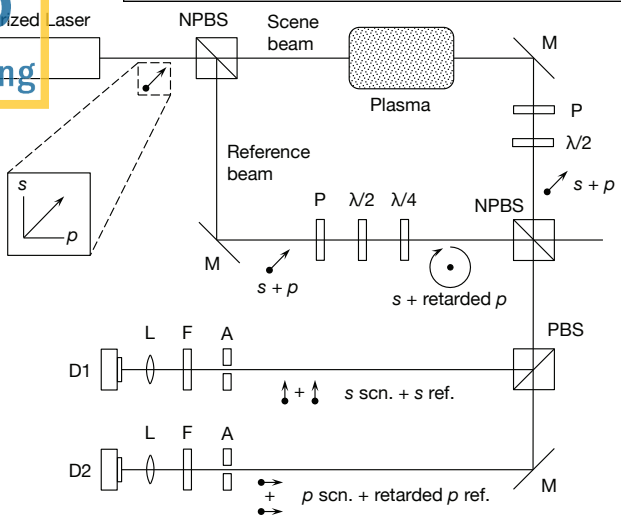

FIG. 1: A simplified schematic of the interferometer and detection scheme, showing the polarization states of the scene, reference, and superposed beams. NPBS denotes a non-polarizing beam splitter, PBS denotes a polarizing beam splitter, M denotes a mirror, P denotes a polarizer, wave plates are denoted by either $\lambda/2$ or $\lambda/4$, A denotes an aperture, F denotes a filter, and L denotes a lens. Detector D1 measures I_s, while D2 measures I_p. The actual system was a two-chord device with additional relay mirrors and vacuum chamber windows.

θ is the phase of the light (i.e., $\theta = \omega t$, where $\omega = 2\pi c/\lambda$ and λ is the laser wavelength, 632.8 nm in this case), ϕ is the variable phase shift due to the plasma plus the constant (over the sub-millisecond experimental timescales) phase shift due to path length differences between the scene and reference beams, and ξ is the imposed phase retardation of the p-polarization component with respect to the *s*-polarization component.

The combined beams can be expressed more simply as

$$\begin{aligned}\mathbf{E}(t) = &\,\mathrm{Re}\left\{\left(\widetilde{E}_{s\,\mathrm{ref}} + \widetilde{E}_{s\,\mathrm{scn}}e^{i\phi}\right)e^{i\theta}\right\}\hat{\mathbf{e}}_\mathbf{s} + \\ &\,\mathrm{Re}\left\{\left(\widetilde{E}_{p\,\mathrm{ref}}e^{i\xi} + \widetilde{E}_{p\,\mathrm{scn}}e^{i\phi}\right)e^{i\theta}\right\}\hat{\mathbf{e}}_\mathbf{p} \qquad (3)\\ = &\,\mathrm{Re}\left\{\widetilde{E}_s(\phi)e^{i\theta}\right\}\hat{\mathbf{e}}_\mathbf{s} + \mathrm{Re}\left\{\widetilde{E}_p(\phi,\xi)e^{i\theta}\right\}\hat{\mathbf{e}}_\mathbf{p} \qquad (4)\end{aligned}$$

where the superposed modulus (e.g., $\widetilde{E}_p$) varies with respect to the relatively slow phase shift imparted by the plasma (ϕ) and the static phase shift imparted by the retarding elements in the system (ξ). The squared magnitude of the superposed modulus (proportional to intensity) can be obtained by multiplying by its complex conjugate.

$$\begin{aligned}|\widetilde{E}_s|^2 &= \widetilde{E}_s\widetilde{E}_s^* \\ &= \widetilde{E}_{s\,\mathrm{ref}}^2 + \widetilde{E}_{s\,\mathrm{scn}}^2 + 2\widetilde{E}_{s\,\mathrm{ref}}\widetilde{E}_{s\,\mathrm{scn}}\cos\phi \qquad (5)\\ |\widetilde{E}_p|^2 &= \widetilde{E}_p\widetilde{E}_p^* \\ &= \widetilde{E}_{p\,\mathrm{ref}}^2 + \widetilde{E}_{p\,\mathrm{scn}}^2 + 2\widetilde{E}_{p\,\mathrm{ref}}\widetilde{E}_{p\,\mathrm{scn}}\cos(\phi-\xi) \qquad (6)\end{aligned}$$

It is clearly necessary to introduce a phase shift to one of the polarization components to achieve quadratic phase detection. A retardation of $\xi = \pi/2$ was applied to the p polarization component of the reference beam through the use of a $\lambda/4$ wave plate, which results in a circularly polarized reference beam. Expressing Eqns. 5 and 6 in terms of intensity (note: $I = \langle S\rangle = \epsilon_o c E_o^2/2$):

$$I_s = I_{s\,\mathrm{ref}} + I_{s\,\mathrm{scn}} + 2\sqrt{I_{s\,\mathrm{ref}}I_{s\,\mathrm{scn}}}\cos\phi \qquad (7)$$

$$I_p = I_{p\,\mathrm{ref}} + I_{p\,\mathrm{scn}} + 2\sqrt{I_{p\,\mathrm{ref}}I_{p\,\mathrm{scn}}}\sin\phi \qquad (8)$$

It is possible to reduce the number of unknowns in Eqns. 7 and 8 by noticing that the ratios $\alpha = I_{s\,\mathrm{ref}}/I_{\mathrm{ref}}$, $\beta = I_{s\,\mathrm{scn}}/I_{\mathrm{scn}}$, $\gamma = I_{p\,\mathrm{ref}}/I_{\mathrm{ref}}$, and $\delta = I_{p\,\mathrm{scn}}/I_{\mathrm{scn}}$ (where, e.g., $I_{\mathrm{ref}} = I_{s\,\mathrm{ref}} + I_{p\,\mathrm{ref}}$) remain constant regardless of laser power fluctuations or attenuation by the object/plasma under investigation ($\alpha+\gamma = \beta+\delta = 1$ at all times, and the ratios α/γ and β/δ are constant). This holds assuming negligible Faraday rotation in the scene beam due to the plasma/object (it should be noted that in the experiments described herein, the plasma conditions are capable of, at most, a few mrad of rotation; in addition, the symmetry of the magnetic geometry along the interferometer line of sight ensures that nearly all Faraday rotation is canceled out). The polarizer placed in the scene beam between the plasma and the recombining beam splitter also enforces this state of polarization. The intensities at each detector (Eqns. 7 and 8) can then be expressed as

$$I_s = \alpha I_{\mathrm{ref}} + \beta I_{\mathrm{scn}} + 2\sqrt{\alpha\beta I_{\mathrm{ref}}I_{\mathrm{scn}}}\cos\phi \qquad (9)$$

$$I_p = \gamma I_{\mathrm{ref}} + \delta I_{\mathrm{scn}} + 2\sqrt{\gamma\delta I_{\mathrm{ref}}I_{\mathrm{scn}}}\sin\phi \qquad (10)$$

where, in this case, $\alpha = \beta = \gamma = \delta = \frac{1}{2}$, corresponding to 45° and circular polarizations in the scene and reference beams respectively. A calibration procedure to properly scale the detector signals to one another is outlined in Appendix A.

In this system, the reference beam intensity remains constant over the timescales of the measurement since it does not pass through the plasma and the laser does not exhibit power variations over such short timescales. However, the scene beam may be attenuated by the plasma and intensity variations must be taken into account. Once the scaled intensities I_s and I_p are known, I_{ref} can be inferred using Eqn. B6 and baseline calibration data as described in Appendix B. The scene beam intensity can then be determined throughout the course of a plasma discharge, regardless of phase or attenuation, in terms of I_{ref}, I_s, and I_p using Eqn. C4,

$$\begin{aligned}I_{\mathrm{scn}} = &I_s + I_p \\ &- \sqrt{2I_{\mathrm{ref}}\left(I_s + I_p\right) - I_{\mathrm{ref}}^2 - \left(I_s - I_p\right)^2}\end{aligned} \qquad (11)$$

provided that $I_{\mathrm{scn}}/I_{\mathrm{ref}} \leq 0.5$ (see Appendix C).

Since I_{ref} does not change during a plasma discharge, and I_{scn} can be computed using the above method, the interferometric phase can be estimated by rearranging Eqns. 9 and 10 to solve for $\cos\phi$ and $\sin\phi$. Using $\alpha = \beta = \gamma = \delta = \frac{1}{2}$,

$$\kappa = \frac{I_s - \frac{1}{2}I_{\mathrm{ref}} - \frac{1}{2}I_{\mathrm{scn}}}{\sqrt{I_{\mathrm{ref}}I_{\mathrm{scn}}}} \qquad (12)$$

$$\sigma = \frac{I_p - \frac{1}{2}I_{\mathrm{ref}} - \frac{1}{2}I_{\mathrm{scn}}}{\sqrt{I_{\mathrm{ref}}I_{\mathrm{scn}}}} \qquad (13)$$

where κ and σ are nominally $\cos\phi$ and $\sin\phi$ respectively. Substituting κ and σ for $\cos\phi$ and $\sin\phi$ in Euler's formula, $e^{i\phi} = \cos\phi + i\sin\phi$, and rearranging:

$$\Phi = \frac{\ln|\kappa + i\sigma|}{i} \tag{14}$$

where the complex quantity Φ is the numerical solution for the phase difference ϕ. The real part of Φ can be taken as an approximation of ϕ, while an estimate of the error in computed phase can be made by considering the difference between the modulus of Φ and the magnitude of the real part.

$$\phi \approx \mathrm{Re}\{\Phi\} \tag{15}$$

$$\text{error} \approx \sqrt{\Phi\Phi^*} - |\mathrm{Re}\{\Phi\}| \tag{16}$$

IV. EXPERIMENTAL RESULTS

A two-chord version of this system (i.e., two complete systems driven by one laser) was fielded on the Magnetized Shock Experiment (MSX)[11–13] at Los Alamos National Laboratory; which produces magnetized, collisionless, supersonic/super-Alfvénic plasma flows with similar dimensionless parameters to those found in both space and astrophysical shocks. During a discharge, a discrete magnetized plasmoid is formed at one end of the experiment, which translates for a short distance, then impacts a static object; in this case, a strong magnetic field embedded in a cloud of neutral gas near a solid conductive wall. The integrated electron density along the path of the beam can be determined by measuring the change in the scene/reference phase difference, ϕ, using[4]

$$\phi = \frac{-\omega}{2cn_c}\int n_e \mathrm{d}l \tag{17}$$

where n_e is the electron density along length element dl, $n_c = \epsilon_o m_e \omega^2/e^2$ is the cutoff density for electromagnetic waves with frequency ω in rad/s, m_e is the electron mass, e is the elementary charge, ϵ_o is the vacuum permittivity, and c is the speed of light. For the 632.8 nm wavelength laser used in the MSX system, $\phi = -1.77\times10^{21}\int n_e \mathrm{d}l$ in SI units. The two interferometry chords are located near to the point of impact with a spacing of a few millimeters to observe the fast dynamics and large density gradients resulting from the stagnation of such flows.

During construction and initial testing, several refinements were made to the system. Initially, it was envisioned that both outputs of the recombining beam splitter would be used in the detection scheme, with each output passed through orthogonal polarizers, enabling the s and p polarization components to be measured. To this end, several different types of non-polarizing beam splitters were tested, including partially silvered plate beam splitters, pellicles, and cube beam splitters. However, all of the tested beam splitters exhibited some degree of polarization dependency in the splitting ratio, and all introduced different amounts of relative phase delay to the polarization components depending on whether the beam was transmitted or reflected. Thus, any interferometric scheme that uses both outputs of a non-polarizing beam splitter must take both the polarization-dependent splitting ratio *and* the difference in phase shift between outputs into account. However, in this case, a different approach was adopted; only one output was utilized, which was subsequently split into s and p components using a polarizing beam splitter.

The laser that was used (Helium-Neon laser operating at 632.8 nm) exhibited intensity modulations at ∼400 MHz, which was near the frequency limit of the digitizers used in the final system (sampling rate of 2.5 GSa/s, analog bandwidth of 300 MHz) and also near the response limit of the silicon photodiodes used (∼1 ns rise-time). Although, conceptually, this approach is capable of nearly unlimited bandwidth, to avoid any potential aliasing or high-frequency response issues while preserving as much system bandwidth as possible, all signals were conditioned using multi-pole low-pass filters (-3 dB roll-off at 210MHz, down to -36dB at 300MHz). The intensity modulations are not problematic from an interference standpoint because the difference in path lengths between the scene and reference beams are not large enough to cause the two beams to interfere at different intensities; the filtered signals are simply the average power of the s and p components. The use of a single longitudinal mode laser would avoid the high-frequency intensity modulations that were observed here and allow for extension to higher bandwidth measurements.

Upon taking initial data, it was immediately found that the plasma emission was overwhelming the signal from the laser. To combat this, pinhole apertures (marked "A" in Fig. 1), lenses (marked "L"), and band-pass filters (10±2 nm FWHM laser line filter centered at 632.8 nm, marked "F") were installed just prior to the detectors to reduce their spatial and spectral acceptance to match the laser. This strategy proved successful and plasma emission was no longer measurable on the detectors during stagnation.

Raw data from one chord during typical discharge are displayed in Fig. 2a (the other chord provided similar quality of data with slight differences due to the different axial position); after an initially quiescent phase, the s and p intensities exhibit a sudden burst of rapid activity, with fringe shifts taking place over timescales as short as 10 ns, followed by a period of relatively slower dynamics. Variations in the maxima and minima of the signal are indicative of attenuation of the scene beam by the plasma. This is reflected in the scene beam intensity, calculated using Eqn. C4 (Fig. 2b), which is reduced by >50% at times. By acquiring data without a plasma present, laser output power was found to be steady over experimental timescales; therefore, monitoring the laser output power during a shot at the cost of introducing an additional detector was deemed unnecessary; however, it should be recognized that since the reference beam intensity is assumed constant, measurement noise manifests in the computed scene beam intensity (which is of relatively little experimental interest in this case). The measured detector signals (Fig. 2a) span roughly 20 arbitrary units (A.U.) of intensity as the phase shifts by π and exhibits ∼1 A.U. of noise in both traces (corresponding to roughly 0.1 – 0.15 radians of phase noise). The noise present in the computed scene beam intensity (Fig. 2b) is of roughly

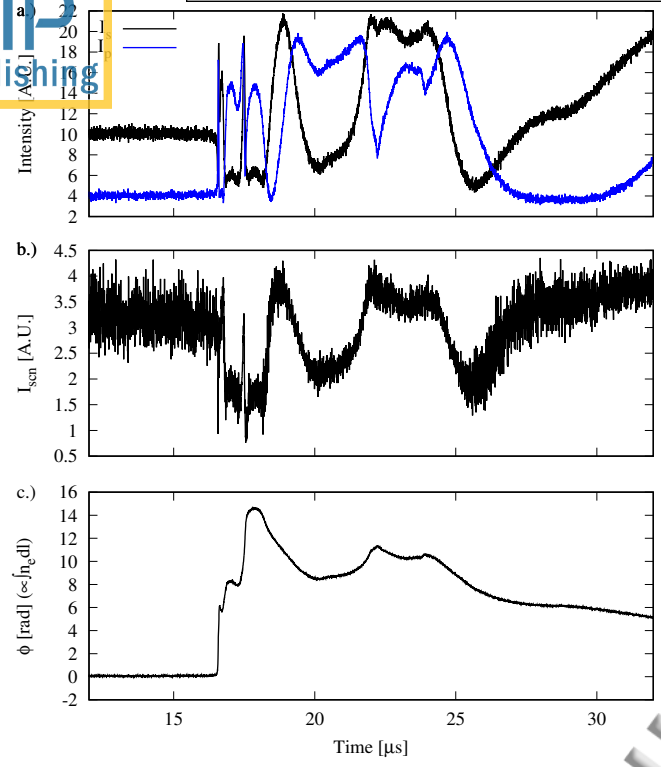

FIG. 2: Data from a typical discharge: (a) measured s and p intensities, (b) computed scene beam intensity, (c) interferometric phase (proportional to chord-averaged plasma density).

the same magnitude (∼1 A.U.).

The interferometric phase (Fig. 2c), proportional to the plasma density integrated along the scene beam (or "chord-averaged" density), exhibits an extremely rapid initial rise with short-timescale structure and overall low levels of noise. Plasma can be seen to arrive after ∼16μs, after which the density increases during the stagnation phase, peaks with a maximum phase shift of approximately 15 radians (or $\int n_e dl \approx 8.5 \times 10^{21}$ m^{-2}), then decreases as the plasma expands back upstream. Framing camera images indicate that the transverse extent of the plasma is a few cm, which implies peak chord-averaged densities on the order of 10^{23} m^{-3}. Note that the phase difference is measured continuously through multiple crossings of π. If plotted on longer timescales, the signal can be seen to return to zero once all the plasma has left the vicinity of the interferometer. Other diagnostics in this section of the experiment included a multichannel soft x-ray Ross filter array with a wide field of view and a visible light framing camera, which both showed increased emission during stagnation qualitatively consistent with the interferometer results. Overall noise levels are on the order of 0.1 radians (corresponding to $\int n dl \approx 5 \times 10^{19}$ m^{-2}), which is consistent with the noise present in the raw signals. Throughout the shot, the level of calculated phase error remained substantially lower that the magnitude of the phase, indicating that this approach is robust to noise and/or uncertainty in measured intensities. Both the bandwidth and the signal/noise ratio of the phase were substantially higher than previously attained in similar experiments using acousto-optic-modulated heterodyne interferometry,[14–16] which could not resolve the fast dynamics taking place over nanosecond timescales.

V. CONCLUSIONS

The interferometer and analysis procedure described herein have been used to measure high-speed (∼10 ns), high-dynamic range (several multiples of π) changes in interferometric phase, corresponding with line-integrated plasma density, in the presence of strong time-dependent attenuation of the scene beam. This was accomplished by using orthogonal polarization components to effectively form two homodyne interferometers with a relative phase shift, resulting in an approach combines the desirable features of both heterodyne and homodyne interferometry; high-bandwidth, high-dynamic range, tolerance to beam power variations.

In this type of system, the number of unknown quantities that can be determined is equal to the number of detectors used. However, since both $\sin\phi$ and $\cos\phi$ are needed to measure phase in quadrature, two detectors are needed at a minimum for the phase measurement, and another unknown, in this case the scene beam intensity, can be obtained for free. With the common availability of stable lasers, it should not be necessary to monitor laser output power even over long timescales; however, if constant laser power over a discharge cannot be assumed (e.g., if a pulsed laser were used), a third detector to measure light split off from the laser output or the reference beam could be added to the system to solve for the three unknowns following a similar mathematical procedure.

If one is free to increase the phase sensitivity, e.g., by using a multi-pass system or by increasing laser wavelength to obtain a larger phase shift for a given plasma density (c.f., Eqn. 17), then the dynamic range of a measurement can be increased provided that the detectors have sufficient time response to track the phase difference through many fringes. In this way, instrument bandwidth can be traded for dynamic range, and the total system bandwidth-dynamic range product is set by the detector speed and signal/noise. During periods of known slow dynamics, higher levels of signal/noise can obtained (at the expense of bandwidth) through signal averaging. Higher laser intensities (e.g., pulsed lasers) could also increases signal/noise at the detectors for increased effective dynamic range. This also enables the use of narrower bandpass laser line filters to overcome higher levels of plasma emission (e.g., in experiments that produce higher density plasmas).

In principle, nearly unlimited bandwidth is possible due to the homodyne nature of this approach (and due to the quadratic nature of the phase measurement, nearly unlimited dynamic range is also possible). By combining this technique with streak camera detection and pulsed lasers, interferometric phase may be tracked in quadrature with sub-picosecond resolution, opening the possibility of interrogating ultra-fast phenomena or probing dense plasmas such as those occurring in high-energy-density physics experiments. Potentially femtosecond

This manuscript was accepted by Rev. Sci.Instrum. Click here to see the version of record.

temporal response is attainable using visible light (frequencies of 100s of THz), with shorter measurement timescales possible if shorter wavelengths are used. With sufficient light source intensity, the ultimate attainable bandwidths and dynamic ranges using this method are, in practice, limited only by available detector technology.

ACKNOWLEDGMENTS

This material is based upon work supported by the U.S. Department of Energy, Office of Science, Office of Fusion Energy Sciences under contract number DE-AC52-06NA25369.

Appendix A: Detector calibration

The signal produced at each detector is proportional to the intensity; e.g., $V_s - V_{so} = \eta_s I_s$, where V_s is the measured voltage of the s detector, V_{so} is the voltage offset (measured by blocking the beams and recording the voltage), and η_s is the detection efficiency including the effects of the optical elements associated with the detectors (aperture, filter, and lens). Mechanical vibrations will typically induce a phase shift such that the intensity maxima and minima can be recorded over the course of tens of milliseconds. Relative detector efficiencies can be determined by acquiring a signal with no plasma present over timescales longer than the characteristic mechanical vibration time of the system, recording the signal maxima and minima, and following the analysis outlined in this section.

Starting with Eqns. 9 and 10, using $\alpha = \beta = \gamma = \delta = \frac{1}{2}$, noting that intensity minima and maxima occur at $\phi = n\pi$ (where $n = 1, 2, 3...$) for the s polarization and $\phi = (n + \frac{1}{2})\pi$ for the p polarization,

$$I_{s\,\max} = \frac{1}{2}I_{\rm ref} + \frac{1}{2}I_{\rm scn} + \sqrt{I_{\rm ref}I_{\rm scn}} \tag{A1}$$

$$I_{s\,\min} = \frac{1}{2}I_{\rm ref} + \frac{1}{2}I_{\rm scn} - \sqrt{I_{\rm ref}I_{\rm scn}} \tag{A2}$$

$$I_{p\,\max} = \frac{1}{2}I_{\rm ref} + \frac{1}{2}I_{\rm scn} + \sqrt{I_{\rm ref}I_{\rm scn}} \tag{A3}$$

$$I_{p\,\min} = \frac{1}{2}I_{\rm ref} + \frac{1}{2}I_{\rm scn} - \sqrt{I_{\rm ref}I_{\rm scn}} \tag{A4}$$

and recalling that, for each polarization $V - V_{\rm o} = \eta I$, one can relate the intensity maxima and minima to the measured voltage maxima and minima without reference to the voltage offset.

$$I_{s\,\max} - I_{s\,\min} = \frac{V_{s\,\max} - V_{s\,\min}}{\eta_s} \tag{A5}$$

Examining Eqns. A1 – A4, note that $I_{s\,\max} = I_{p\,\max}$, $I_{s\,\min} = I_{p\,\min}$, and therefore $I_{s\,\max} - I_{s\,\min} = I_{p\,\max} - I_{p\,\min}$. Thus the efficiency η_p can be expressed as a function of η_s and the voltage swing.

$$\frac{V_{s\,\max} - V_{s\,\min}}{\eta_s} = \frac{V_{p\,\max} - V_{p\,\min}}{\eta_p} \tag{A6}$$

Since a scaling factor would not effect the determination of the phase, only the ratio η_s/η_p is needed, thus $\eta_s = 1$ can be defined and the corresponding η_p can be determined using Eqn. A6.

A similar approach can be used to determine one detector offset in terms of the other if the efficiencies η_s and η_p are known using, for example, $I_{s\,\min} = I_{p\,\min}$.

$$\frac{V_{s\,\min} - V_{s\,\rm o}}{\eta_s} = \frac{V_{s\,\min} - V_{s\,\rm o}}{\eta_p} \tag{A7}$$

However, this approach to determining the offset was not used for the data in this paper as it was trivial to measure both offsets independently.

Calibration data were typically taken at the beginning and end of each shot day, and sometimes periodically throughout the day. The detection efficiencies, voltage offsets, and beam intensities were not observed to change appreciably over the course of several days, however, occasional realignment was performed on the system to maximize the recorded signal.

Appendix B: Reference beam intensity

The scene/reference beam intensity ratio, $I_{\rm ratio} = I_{\rm scn}/I_{\rm ref}$, does not change with variations in laser power and can be used to determine the reference beam intensity, $I_{\rm ref}$, without disassembling the interferometer using the same calibration data used to determine the detector efficiencies. This is critical because disassembly and reassembly of the system would alter the alignment, which would alter both the intensity ratio and the detector system efficiencies. It also allows the diagnostician to periodically acquire calibration data to check for changes in alignment and monitor laser power without requiring entry into the experimental bay.

Using, for example, the s-polarization, Eqns. A1 and A2 can be rewritten as

$$\frac{I_{s\,\max}}{I_{\rm ref}} = \frac{1}{2} + \frac{1}{2}I_{\rm ratio} + \sqrt{I_{\rm ratio}} \tag{B1}$$

$$\frac{I_{s\,\min}}{I_{\rm ref}} = \frac{1}{2} + \frac{1}{2}I_{\rm ratio} - \sqrt{I_{\rm ratio}} \tag{B2}$$

Noticing that

$$\frac{I_{s\,\max} + I_{s\,\min}}{I_{s\,\max} - I_{s\,\min}} = \frac{I_{\rm ratio} + 1}{2\sqrt{I_{\rm ratio}}} \tag{B3}$$

allows $I_{\rm ratio}$ to be calculated in terms of only the measured intensity maxima and minima. Furthermore, the substitution

$$\xi = 2\left(\frac{I_{s\,\max} + I_{s\,\min}}{I_{s\,\max} - I_{s\,\min}}\right)^2 - 1 \tag{B4}$$

allows $I_{\rm ratio}$ to be expressed simply as

$$I_{\rm ratio} = \xi \pm \sqrt{\xi^2 - 1} \tag{B5}$$

The sign of the second term can be easily determined by checking whether $I_{\rm ratio} > 1$ or < 1 by blocking either of

the beams and recording the photodiode output voltage. It should be noted that the same approach can be used with the p-polarization as well, which may be useful as a check.

Combining Eqns. B1 and B2, I_{ref} can be expressed as a function of I_{ratio} and the s-polarization intensity variation.

$$I_{\text{ref}} = \frac{I_{s\,\max} - I_{s\,\min}}{2\sqrt{I_{\text{ratio}}}} \tag{B6}$$

It is interesting to note that expressing Eqns. 9 and 10 in terms of I_{ratio} and I_{ref}, using $\alpha = \beta = \gamma = \delta = 1/2$, and rearranging,

$$\cos\phi = \frac{2I_s - I_{\text{ref}}I_{\text{ratio}} - I_{\text{ref}}}{2\sqrt{I_{\text{ref}}^2 I_{\text{ratio}}}} \tag{B7}$$

$$\sin\phi = \frac{2I_p - I_{\text{ref}}I_{\text{ratio}} - I_{\text{ref}}}{2\sqrt{I_{\text{ref}}^2 I_{\text{ratio}}}} \tag{B8}$$

then combining these equations using the trigonometric identity $\sin^2\phi + \cos^2\phi = 1$,

$$\frac{(2I_s - I_{\text{ref}}I_{\text{ratio}} - I_{\text{ref}})^2}{4I_{\text{ref}}^2 I_{\text{ratio}}} + \frac{(2I_p - I_{\text{ref}}I_{\text{ratio}} - I_{\text{ref}})^2}{4I_{\text{ref}}^2 I_{\text{ratio}}} = 1 \tag{B9}$$

and finally solving for I_{ref} yields

$$I_{\text{ref}} = \frac{1}{I_{\text{ratio}}^2 + 1}\left[(I_s + I_p)(I_{\text{ratio}} + 1) \pm \sqrt{2(I_s + I_p)^2 I_{\text{ratio}} - (I_s - I_p)^2(I_{\text{ratio}}^2 + 1)}\right] \tag{B10}$$

Naïvely, it appears possible to determine I_{ref} as a function of a predetermined I_{ratio} and measured I_s and I_p at the beginning of a discharge, before plasma shows up to potentially alter I_{scn} and by extension I_{ratio}. However, the sign of the second term in parentheses is ambiguous, with the "plus" and "minus" signs alternately providing the correct value for I_{ref} depending on the phase regardless of the value of I_{ratio}. Unfortunately, without *a priori* knowledge of the phase, this approach cannot be used to determine I_{ref} prior to the arrival of the plasma. One is therefore forced to assume a constant reference beam intensity shot to shot (which, in this case, is a valid assumption).

Appendix C: Scene beam intensity

The scene beam intensity can be determined over the course of a plasma discharge using a known reference beam intensity. Rearranging Eqns. 9 and 10 with $\alpha = \beta = \gamma = \delta = \frac{1}{2}$,

$$\cos\phi = \frac{I_s - \frac{1}{2}I_{\text{ref}} - \frac{1}{2}I_{\text{scn}}}{\sqrt{I_{\text{ref}}I_{\text{scn}}}} \tag{C1}$$

$$\sin\phi = \frac{I_p - \frac{1}{2}I_{\text{ref}} - \frac{1}{2}I_{\text{scn}}}{\sqrt{I_{\text{ref}}I_{\text{scn}}}} \tag{C2}$$

and using the trigonometric identity $\sin^2\phi + \cos^2\phi = 1$,

$$\frac{\left(I_s - \frac{1}{2}I_{\text{ref}} - \frac{1}{2}I_{\text{scn}}\right)^2}{I_{\text{ref}}I_{\text{scn}}} + \frac{\left(I_p - \frac{1}{2}I_{\text{ref}} - \frac{1}{2}I_{\text{scn}}\right)^2}{I_{\text{ref}}I_{\text{scn}}} = 1 \tag{C3}$$

I_{scn} can be expressed in terms of the known reference beam intensity and the measured s and p intensities.

$$I_{\text{scn}} = I_s + I_p \pm \sqrt{2I_{\text{ref}}(I_s + I_p) - I_{\text{ref}}^2 - (I_s - I_p)^2} \tag{C4}$$

The sign ambiguity of the last term is a result of the symmetry of the equations 9 and 10 about I_{scn} and I_{ref}. If $I_{\text{ratio}} > 0.5$ ($I_{\text{ratio}} = I_{\text{scn}}/I_{\text{ref}}$, see Appendix B), either the "plus" or "minus" signs provide the correct scene beam intensity depending on I_{ratio} and the phase, similar to the sign ambiguity in Eqn. B10. Fortunately however, for $I_{\text{ratio}} \leq 0.5$, the minus sign provides the correct value for the scene beam intensity at any phase. Attenuation of the scene beam can be easily achieved using a neutral density filter, however, the additional relay mirrors and vacuum chamber windows in the scene beam attenuate I_{scn} to a degree that the condition $I_{\text{ratio}} \leq 0.5$ is satisfied in this case.

[1] P. Hariharan. *Optical Interferometry*. Academic Press, 2 edition, 2003.

[2] Stephen Mitchell Wolfe, KJ Button, J Waldman, and DR Cohn. Modulated submillimeter laser interferometer system for plasma density measurements. *Applied optics*, 15(11):2645–2648, 1976.

[3] D Veron. High sensitivity hcn laser interferometer for plasma electron density measurements. *Optics Communications*, 10(1):95–98, 1974.

[4] Ian H Hutchinson. *Principles of plasma diagnostics*. Cambridge university press, 2005.

[5] DH Martin and E Puplett. Polarised interferometric spectrometry for the millimetre and submillimetre spectrum. *Infrared Physics*, 10(2):105–109, 1970.

[6] GMB Bouricius and SF Clifford. An optical interferometer using polarization coding to obtain quadrature phase components. *Review of Scientific Instruments*, 41(12):1800–1803, 1970.

[7] CJ Buchenauer and AR Jacobson. Quadrature interferometer for plasma density measurements. *Review of Scientific Instruments*, 48(7):769–774, 1977.

[8] Vincenzo Greco, Giuseppe Molesini, and Franco Quercioli. Accurate polarization interferometer. *Review of scientific instruments*, 66(7):3729–3734, 1995.

[9] Xinqun Liu, Warwick Clegg, David FL Jenkins, and Bo Liu. Polarization interferometer for measuring small displacement. *Instrumentation and Measurement, IEEE Transactions on*, 50(4):868–871, 2001.

[10] TaeBong Eom, JongYun Kim, and Kyuwon Jeong. The dynamic compensation of nonlinearity in a homodyne laser interferometer. *Measurement Science and Technology*, 12(10):1734, 2001.

[11] TE Weber, RJ Smith, and SC Hsu. Laboratory studies of magnetized collisionless flows and shocks using accelerated plasmoids. *Bulletin of the American Physical Society*, 60, 2015.

[12] RJ Smith and TE Weber. A streak camera based fiber optic pulsed polarimetry technique for magnetic sensing to sub-mm resolution. *Review of Scientific Instruments*, 87(11):11E725, 2016.

[13] TE Weber, TP Intrator, and RJ Smith. Plasma-gun-assisted field-reversed configuration formation in a conical θ-pinch. *Physics of Plasmas (1994-present)*, 22(4):042518, 2015.

[14] TE Weber, RJ Smith, TM Hutchinson, SF Taylor, and SC Hsu. First results of transcritical magnetized collisionless shock studies on msx. In *APS Meeting Abstracts*, volume 1, page 8063P, 2014.

[15] C Grabowski, JH Degnan, DJ Amdahl, R Delaney, M Domonkos, FM Lehr, R Magallanes, PR Robinson, EL Ruden, W White, et al. Frc lifetime studies for the field reversed configuration

heating experiment (frchx). In *Pulsed Power Conference (PPC), 2011 IEEE*, pages 431–436. IEEE, 2011.

[16] JH Degnan, DJ Amdahl, M Domonkos, FM Lehr, C Grabowski, PR Robinson, EL Ruden, WM White, GA Wurden, TP Intrator, et al. Recent magneto-inertial fusion experiments on the field reversed configuration heating experiment. *Nuclear Fusion*, 53(9):093003, 2013.

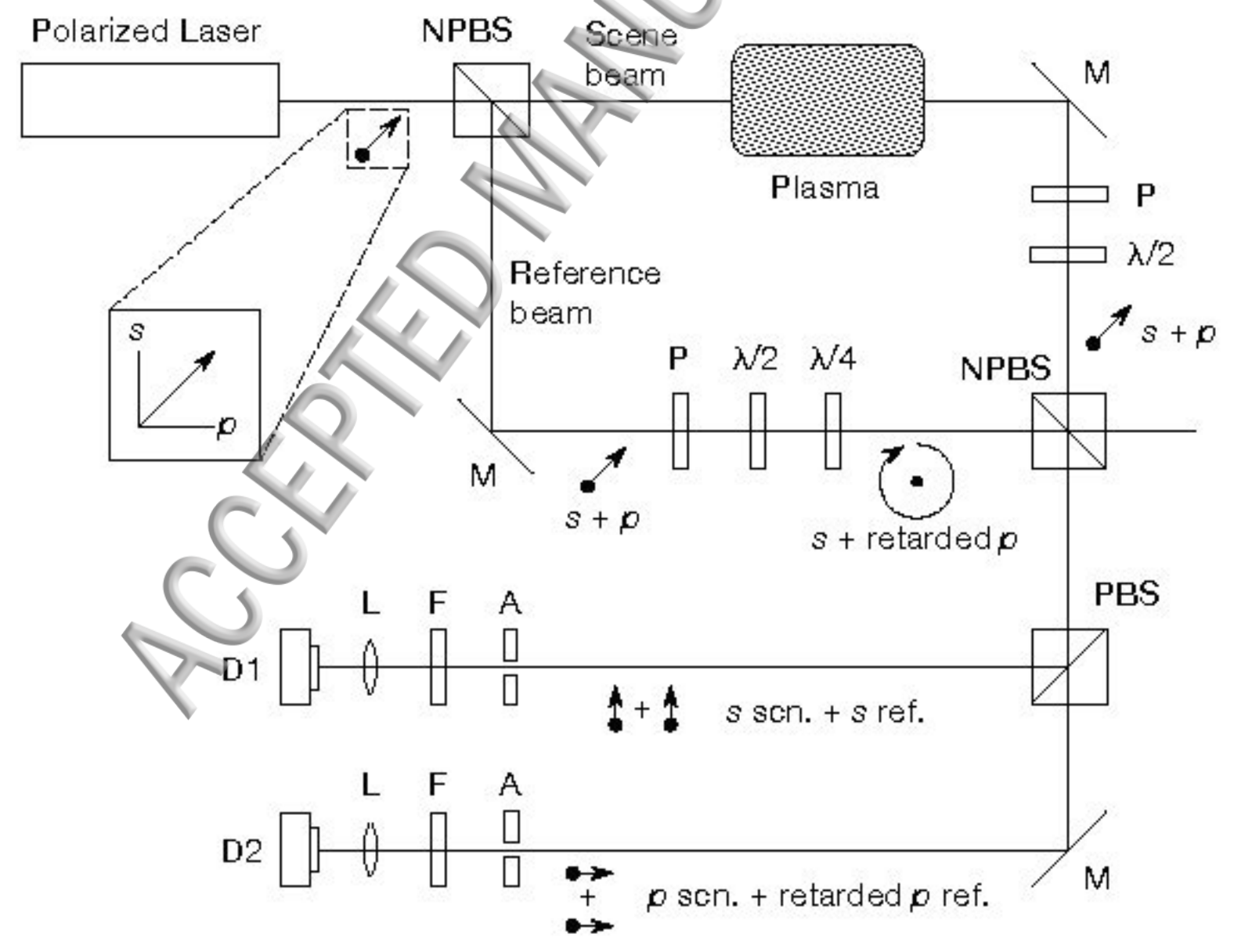

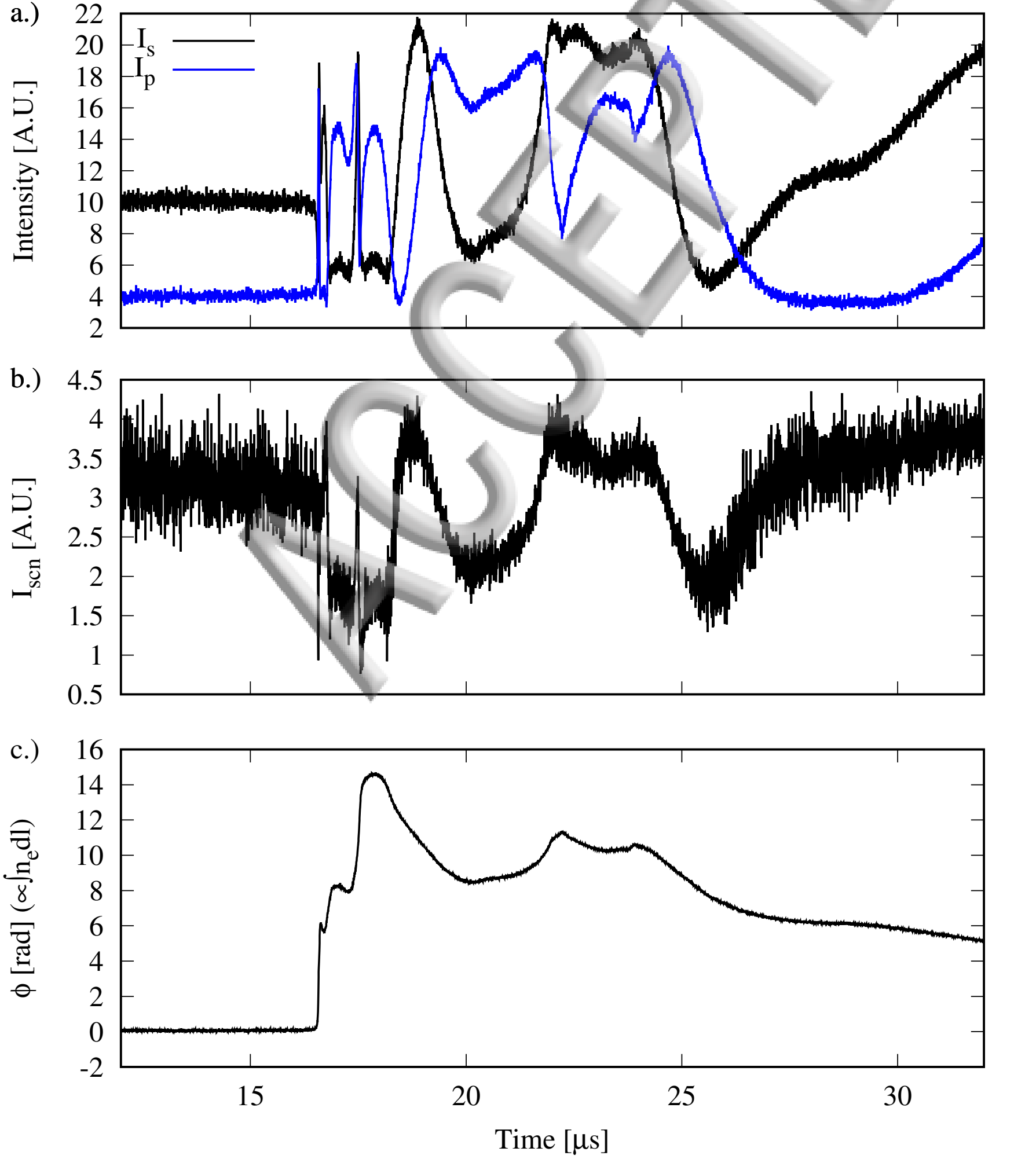
a.)
Intensity [A.U.]
I_s
I_p
22
20
18
16
14
12
10
8
6
4
2
b.)
I_{scn} [A.U.]
4.5
4
3.5
3
2.5
2
1.5
1
0.5
c.)
ϕ [rad] ($\propto\int n_e dl$)
16
14
12
10
8
6
4
2
0
-2
15
20
25
30
Time [μs]